Int J Thermophys (2016) 37:118
DOI 10.1007/s10765-016-2129-y

ICPPP 18

Assessment of the Nucleus-to-Cytoplasmic Ratio in MCF-7 Cells Using Ultra-high Frequency Ultrasound and Photoacoustics

M. J. Moore[1,2,3] · **E. M. Strohm**[1,2,3] · **M. C. Kolios**[1,2,3]

Received: 10 October 2015 / Accepted: 4 October 2016 / Published online: 14 October 2016

Abstract The nucleus-to-cytoplasmic (N:C) ratio of a cell is often used when assessing histology for the presence of malignant disease. In this proof of concept study, we present a new, non-optical method for determination of the N:C ratio using ultra-high Frequency ultrasound (US) and photoacoustics (PA). When using transducers in the 100 MHz–500 MHz range, backscattered US pulses and emitted PA waves are encoded with information pertaining to the dimension and morphology of micron-sized objects. If biological cells are interrogated, the diameter of the scattering or absorbing structure can be assessed by fitting the power spectra of the measured US or PA signals to theoretical models for US backscatter and PA emission from a fluid sphere. In this study, the cell and nucleus diameters of 9 MCF-7 breast cancer cells were determined using a new simplified model that calculates the theoretical values of the location of the power spectra minima for both US and PA signals. These diameters were then used to calculate the N:C ratio of the measured cells. The average cell diameter determined by US pulses from a transducer with a central frequency of 375 MHz was found to be $15.5\,\mu\text{m} \pm 1.8\,\mu\text{m}$. The PA waves emitted by the cell nuclei were used to determine an average nuclear diameter of $12.0\,\mu\text{m} \pm 1.3\,\mu\text{m}$. The N:C ratio for these cells was calculated to be 1.9 ± 1.0, which agrees well with previously reported N:C values for this cell type.

Selected Papers of the 18th International Conference on Photoacoustic and Photothermal Phenomena.

✉ M. C. Kolios
mkolios@ryerson.ca

1 Department of Physics, Ryerson University, Toronto, ON, Canada

2 Institute for Biomedical Engineering, Science and Technology (iBEST), Ryerson University and St. Michaels Hospital, Toronto, ON, Canada

3 Keenan Research Centre for Biomedical Science, St. Michaels Hospital, Toronto, ON, Canada

Keywords Biological cell · Photoacoustic microscopy · Quantitative photoacoustics · Quantitative ultrasound · Ultra-high frequency ultrasound

1 Introduction

Cancer is one of the leading causes of death worldwide, claiming the lives of over 8.2 million people in the year 2012 [1]. The current gold standard for diagnosis of cancerous disease is histological assessment of a biopsy sample via optical microscopy [2]. One of the most prominent features of cancerous cells is an enlarged nucleus due to an atypically large amount of chromatin. The nucleus-to-cytoplasmic (N:C) ratio, defined as the ratio of the cross-sectional area of the nucleus divided by that of the cytoplasm, is a commonly used parameter in tumor staging and grading. Historically the N:C ratio has been assessed qualitatively by pathologists using optical microscopy; however, in recent years several quantitative methods utilizing image recognition software and digital post-processing have been developed to automate the process [3–6]. Even with these advances, the assessment of the cell N:C ratio may be difficult due to the thin tissue samples typically examined. For example, if the tissue slice is not taken through the plane of the cell which exhibits the largest nucleus cross-section, stereological methods must be used to infer the maximum possible nucleus diameter and calculate the N:C ratio. To remediate this, 3D imaging techniques can be used to fully assess cellular and nuclear morphology. Balasubramanian et al. [7] examined circulating tumor cells with confocal microscopy and were able to differentiate malignant and benign cells by their N:C ratios and cytokeratin expression profiles. Nandakumar et al. [8] used the Cell-CT device to obtain 3D images of breast cancer cells and calculate N:C ratios without having to stitch together multiple planar images as in confocal microscopy. However, due to the lengthy imaging time of one cell per minute [9], the Cell-CT device is not suited to the analysis of large cell populations.

A more rapid determination of cell and organelle morphology is possible with flow cytometry (FC) techniques. In conventional FC, forward scattered light is correlated with overall cell size and side scattered light with the cell granularity; however, exact morphological dimensions are not obtained. On the other hand, imaging flow cytometry (IFC) can be used to simultaneously acquire brightfield, darkfield, and fluorescence images of suspended cells at a rate of several hundred cells per second [10–12]. Basiji et al. [12] used the ImageStream IFC system to analyze both normal mammary epithelial cells and mammary carcinoma cells, finding that while the cellular and nuclear areas of the analyzed normal and carcinoma cells was similar, on average the cytoplasmic area of the carcinoma cells was substantially lower than that of the normal cells. In contrast to the in vitro FC and IFC techniques, photothermal flow cytometry (PTFC) and photoacoustic flow cytometry (PAFC) can both be used to interrogate cells in vivo. Zharov et al. have used PTFC for high throughput in vivo imaging of unlabeled erythrocytes and leukocytes in the blood and lymph [13–15]. PAFC on the other hand has been used for the in vivo detection of unlabeled circulating melanoma cells as well as breast cancer cells labeled with gold and magnetic nanoparticles [16–19]. While these techniques have the clear advantage of speed, they

share disadvantages with standard 2D imaging modalities as they do not inherently assess 3D structure.

Recently, ultra-high frequency ultrasound (US) and photoacoustic (PA) methods have been used to assess the morphological structure of single cells [20–22]. At frequencies in the hundreds of megahertz (MHz), the wavelength of the incident US pulse is on the order of the cell diameter, and backscattered US waves contain information about cell size and morphology. This information has previously been extracted from various cell types, including melanoma cells, leukocytes, and erythrocytes [21,23]. A similar phenomenon occurs in PA; when irradiated by a laser, waves generated by the transient thermoelastic expansion are encoded with information pertaining to the size and morphology of the optically absorbing structure [24,25]. Deviations in these PA signals have been used to monitor the change in erythrocyte morphology as a function of the osmolality in the surrounding fluid [23]. In mouse melanoma cells, where the acoustically scattering and optically absorbing volumes are similar, the cell size calculated from backscattered US pulses was found to be in good agreement with cell size extracted from PA signals generated by melanin particles within the cell cytoplasm [21].

In this study, a new mathematical formulation is derived to extract morphological information from the unique features in the US and PA power spectra. This formulation was used to obtain the diameter of MCF-7 breast cancer cells from backscattered ultra-high frequency US pulses and the diameter of the MCF-7 cell nuclei using PA signals originating from the nucleus. These two measurements, when performed on the same cell, can be used to rapidly determine the N:C ratio without the need for optical assessment or stereology.

2 Theory

2.1 Acoustic Scattering by a Fluid Sphere

Biological cells in suspension are approximately spherical and, being composed predominantly of water, have elastic properties determined by their cytoplasm [26]. The theory describing scattering of an acoustic wave by a fluid-filled sphere immersed in liquid was first developed by Anderson in 1950 [27]. In subsequent years, Frey and Goodman simplified the Anderson model for the case of a weakly scattering sphere, i.e., a fluid sphere with acoustic properties approximately the same as those of the surrounding liquid. In this case, the displacement potential arising from the backscattered pulse is given by [28]:

$$\phi(k) = -\frac{\exp(-ikr)}{2kr}(ka)^2(\epsilon + \delta)\, j_1(2ka), \tag{1}$$

where $j_1(z)$ is a spherical Bessel function of the first kind of order one, a is the radius of the fluid sphere, k is the wavenumber of the incident US pulse, r is the distance between the sphere and point at which the acoustic wave is assessed, and ϵ and δ are the percent differences between the bulk moduli and density of the sphere fluid and

surrounding liquid, respectively. Writing Eq. 1 in terms of frequency, it can be shown that the location of minima and maxima in the power spectrum of the backscattered wave are predicted by the zeros and maxima of

$$\Phi(f) = j_1\left(\frac{4\pi a}{v_s} f\right), \tag{2}$$

where v_s is the longitudinal speed of sound within the sphere and f is the frequency. Thus, if the speed of sound within a weakly scattering sphere, e.g., a cell, is known, the radius of the sphere may be approximated by fitting the maxima and minima in the experimentally measured power spectrum to Eq. 2.

2.2 Photoacoustic Signal from a Spherical Absorber

As the acoustic properties of a fluid sphere approach those of the surrounding medium, the PA wave produced by the sphere attains a characteristic N shape described by [29]:

$$p(t) = \frac{r + v_s t}{2r} p_o(r + v_s t) + \frac{r - v_s t}{2r} p_o(-r + v_s t) + \frac{r - v_s t}{2r} p_o(r - v_s t), \tag{3}$$

where a, v_s, and r are as defined in the previous section, and $p_o = p_i U(r) U(-r + a)$; where $U(r)$ is the Heaviside function and p_i is the initial pressure within the sphere. For times $t > \frac{a}{v_s}$ after laser absorption, Eq. 3 can be written as

$$p(t) = \frac{(r - v_s t)}{2r} p_i \Pi\left(\frac{v_s}{2a}\left(t - \frac{r}{v_s}\right)\right), \tag{4}$$

where $\Pi(x)$ is the rect function. An expression for the pressure in the frequency domain of the waveform described by Eq. 4 is obtained via the convolution theorem as follows. The Fourier transform of the first term in the product is

$$\mathcal{F}\left\{\frac{(r - v_s t)}{2r}\right\}(f) = \frac{\delta(f)}{2} - \frac{i v_s}{4\pi r}\frac{\mathrm{d}\delta(f)}{\mathrm{d}f} \tag{5}$$

where $\delta(f)$ is the Dirac delta function. The Fourier transform of the second term is

$$\mathcal{F}\left\{p_i \Pi\left(\frac{v_s}{2a}\left(t - \frac{r}{v_s}\right)\right)\right\}(f) = \frac{p_i \exp\left(-\frac{i2\pi r}{v_s} f\right) \sin\left(\frac{2\pi a}{v_s} f\right)}{\pi f}. \tag{6}$$

Convolution of Eqs. 5 and 6 yields

$$P(f) = -\frac{p_i v_s i}{4\pi^2 f^2 r} \exp\left(-\frac{i2\pi r}{v_s} f\right)\left(\frac{2\pi a f}{v_s}\cos\left(\frac{2\pi a f}{v_s}\right) - \sin\left(\frac{2\pi a f}{v_s}\right)\right), \tag{7}$$

which is equivalent to the model derived by Diebold and Westervelt [30] for a fluid droplet with acoustic properties identical to those of the surrounding liquid. Using the identity

$$j_1(z) = \frac{\sin(z)}{z^2} - \frac{\cos(z)}{z} \tag{8}$$

Eq. 7 can be rewritten in terms of spherical Bessel functions as

$$P(f) = \frac{ip_i a^2}{v_s r} \exp\left(-\frac{i2\pi r}{v_s} f\right) j_1\left(\frac{2\pi a}{v_s} f\right) \tag{9}$$

The radius of optically absorbing liquid spheres can be determined by fitting the power spectra of emitted PA waves to Eq. 9.

3 Methods

3.1 Preparation of the Sample

MCF-7 cells were cultured in phenol red-free Dulbecco's modified Eagle's medium (DMEM) containing 10 % fetal bovine serum by volume. When confluent, cells were trypsinized and resuspended in DMEM. The suspension was incubated in the dark at room temperature for 15 min with DRAQ5, a supravital fluorescent dye used to stain cell nuclei. The absorption of visible light by cell nuclei is negligible; however, DRAQ5 absorbs within the visible spectrum and facilitated the generation of PA signals from the cell nuclei. The stained MCF-7 cells were then suspended in a DMEM solution containing 16 % HEPES buffer solution by volume and transferred to a glass-bottomed petri dish (MatTek, USA). A thin layer of 1 % agar was deposited onto the glass-bottomed dish and allowed to solidify prior to addition of the cells, ensuring that acoustic reflections from the glass did not interfere with forward traveling acoustic waves. The petri dish containing the cells was placed in a climate-controlled enclosure at 37 °C and was allowed to equilibrate with the ambient temperature before measurement.

3.2 System Setup and Measurement

A modified scanning acoustic microscope (Kibero GmbH, Germany) consisting of an inverted optical microscope and translation stage was outfitted with a pulsed 532 nm laser and high-frequency US transducer. The laser had a 330-ps pulse width and 4-kHz repetition rate (Teem Photonics Inc., France), and the ultrasonic transducer had a central frequency of 375 MHz with a −6 dB bandwidth of 150 MHz (Kibero GmbH, Germany). The laser was directed into the microscope optical path and focused onto the sample cells by a 10X optical objective (Olympus, Japan). The theoretical 3-dB acoustic beam diameter at the transducer focus was approximately 4 μm [31], while the $1/e^2$ diameter of the objective focused Gaussian laser beam was approximately

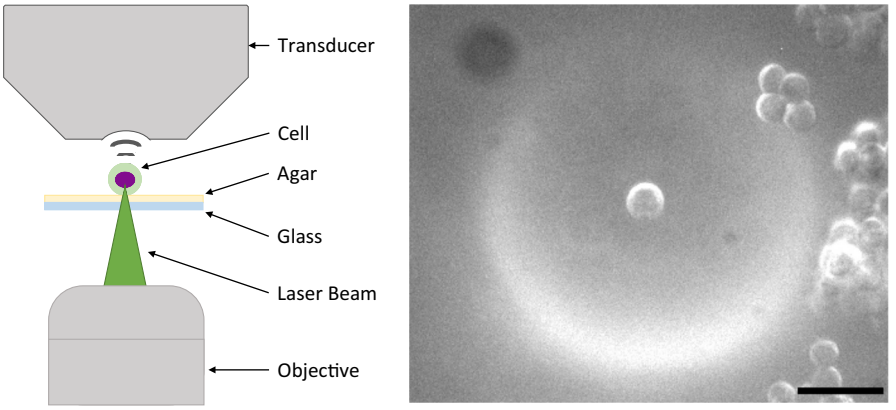

Fig. 1 *Left* Schematic of the experiment setup. *Right* Optical image of a suspended MCF-7 cell, with the transducer cavity faintly visible in the background. The *scale bar* is 40 μm

2 μm [32]. During measurement, the optical objective was slightly defocused to a size of approximately 10 μm to allow irradiation of the entire cell nucleus. The transducer was coaxially aligned to the optical objective on the opposing side of the sample. For each interrogated cell, the backscattered US signals from the cell were recorded first, and then, PA signals were acquired from the nucleus. A schematic of the system and a cross-sectional view through the microscope optics are shown in Fig. 1.

3.3 Signal Processing

Acquired US and PA A-lines were digitized using a 10-bit digitizer with an 8 GHz sampling frequency (DC252, Acqiris, USA). Acquired A-lines were averaged 200 times to increase the signal-to-noise ratio (SNR) and were time-gated so that they contained only the desired signal. A Hamming window with length equal to that of the time-gated signal was applied prior to zero-padding and fast Fourier transformation of the signal in MATLAB. A peak detection algorithm was used to locate maxima and minima in the normalized power spectra. These extrema were then used to determine a set of possible values for the radius, a, using Eqs. 2 and 9 for the cell and nucleus, respectively. The value of a that yielded the theoretical fit with the lowest root mean square error compared to the measured spectra was taken as the radius. In the fitting process it was assumed that the speed of sound was 1575 m s^{-1} for all measured cells [33]. Finally, the N:C ratio was calculated as:

$$\text{N:C} = \frac{N}{C - N}, \tag{10}$$

where N is the cross-sectional area of the nucleus and C is the cross-sectional area of the cell. All cross-sectional areas were calculated based on the radii obtained by the fitting algorithm.

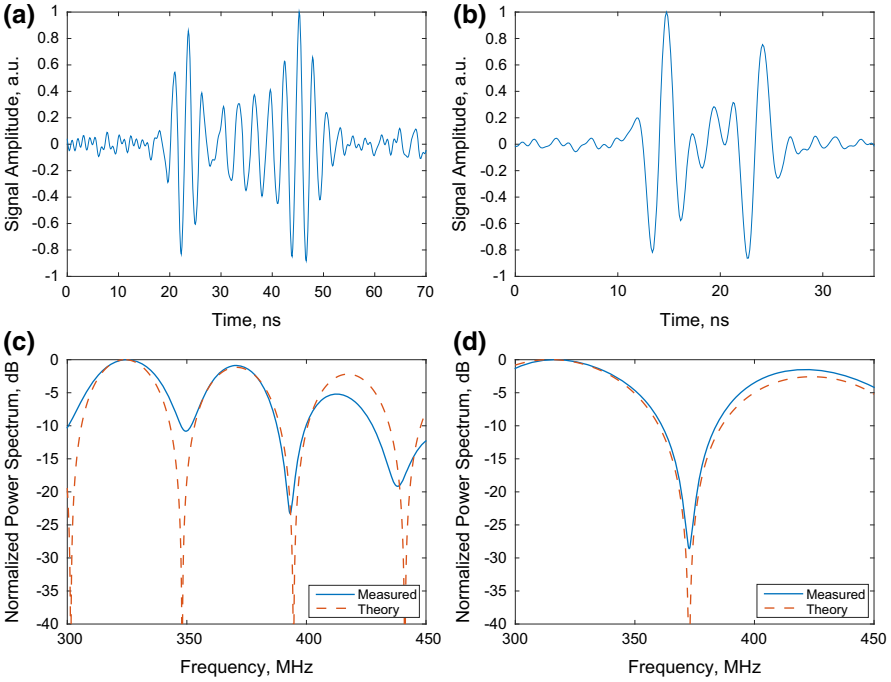

Fig. 2 Measured A-lines from an US pulse backscattered by a cell (a) and PA signal emitted by the nucleus of the same cell (b). The power spectra of the backscattered US pulse and the best-fit spectrum generated using Eq. 2 and photoacoustic signal and the fit power spectrum of Eq. 9 are shown in (c, d), respectively. The power spectra were windowed to match the transducer bandwidth

4 Results and Discussion

For this proof of concept study, 9 cells were interrogated: first with US and subsequently with PA. All measured signals were fit using the algorithm described in the previous section. Representative measured US and PA signals acquired from the same cell as well as the corresponding calculated and fit power spectra are shown in Fig. 2.

The US and PA spectral fitting techniques described in this work are sensitive to the assumed speed of sound within the cell and nucleus, respectively. The locations of the extrema predicted by Eqs. 2 and 9 are unique with respect to the argument a/v_s. Therefore, for a fixed value of v_s, there exists only one a which will yield the detected extrema in the measured signal power spectrum. Thus, there is an intrinsic uncertainty in a due to uncertainty in the assumed value of v_s. In previous studies, the standard deviation in the speed of sound of MCF-7 cells throughout various phases of their cell cycle was found to be less than 1.5 % of the mean calculated sound speed [33,34]. Therefore, an unstated uncertainty of 1.5 % in each of the calculated values of a in this work can be assumed.

The time-domain US signal and its power spectrum are shown in Fig. 2a,c, respectively, along with the closest matching analytical solution fit using Eq. 2. Good agreement is observed between the locations of the spectral minima and maxima

in both the measured and analytical power spectra. The average cell diameter determined using the US backscatter fitting process was 15.5 μm ± 1.8 μm. This is in good agreement with the reported MCF-7 cellular diameter of 16.2 μm ± 3.0 μm found by Reile et al. [35]. Other studies have reported larger average MCF-7 diameters of 18 μm ± 2.0 μm [36] and 19.1 μm ± 8.4 μm [37]. Factors such as the type of growth medium and number of passages may be responsible for the variation in the reported MCF-7 diameters.

The PA power spectrum in Fig. 2d was obtained by applying a Fourier transform to the measured PA signal shown in Fig. 2b. The best-fit power spectrum generated using Eq. 9 is shown in orange in Fig. 2d. The average nucleus diameter as determined by fitting of the PA spectra originating from the stained nuclei was 12.0 μm ± 1.3 μm, which is comparable to the value of 9.2 μm ± 2.9 μm reported by Dahle et al [38]. The average calculated N:C ratio calculated using Eq. 10 was 1.9 ± 1.0. This is in good agreement with the published N:C value of 1.8 ± 0.2 for the MCF-7 cell line [39]. For cells with an N:C ratio of 1.9 %, 53 % of the cell volume is occupied by the nucleus. In comparison, the nucleus of eukaryotic cells typically occupies 10 % of the total cell volume [40].

In this proof of concept study, the cell size, nucleus size, and N:C ratio of MCF-7 breast cancer cells were calculated by comparing measured US and PA power spectra to simplified theoretical equations. This measurement method could aid pathologists in detection and classification of malignant and non-malignant cells in a blood or biopsy sample.

5 Conclusion

A method for assessing the size of cells and cell nuclei as well as the N:C ratio using high-frequency US and PA has been developed. Simple analytical solutions were derived for the rapid determination of the US and PA signal power spectra minima and maxima. The mean cell and nucleus diameter for MCF-7 cells were calculated to be 15.5 μm ± 1.8 μm and 12.0 μm ± 1.3 μm, respectively. The mean calculated N:C ratio of 1.9 ± 1.0 was consistent with other published data. In the future, this technique, which does not require optical imaging of sample cells, will be integrated into the software of a US/PA flow cytometer [41] and used to analyze blood samples for the presence of cancerous cells.

Acknowledgments The authors would like to thank E. Berndl (Ryerson University) for her assistance with biological cell culturing. This research is supported in part by the Natural Sciences and Engineering Research Council of Canada, the Canadian Cancer Society, the Canadian Foundation for Innovation, and the Ontario Ministry for Research and Innovation.

References

1. B. Stewart, C. Wild, *World Cancer Report 2014* (International Agency for Research on Cancer, Lyon, 2014)
2. C. Fletcher, *Diagnostic Histopathology of Tumors*, 4th edn. (Saunders/Elsevier, Philadelphia, 2013)
3. J.A. Swanson, M. Lee, P.E. Knapp, J. Cell Biol. **115**, 941 (1991). doi:10.1083/jcb.115.4.941

4. M.J. Doughty, Curr. Eye Res. **37**, 583 (2012). doi:10.3109/02713683.2012.655397
5. E. Cosatto, M. Miller, H.P. Graf, J.S. Meyer, Pattern Recognition, 2008. *ICPR 2008. In 19th International Conference* pp. 1–4 (2008). doi:10.1109/ICPR.2008.4761112
6. S. Petushi, F.U. Garcia, M.M. Haber, C. Katsinis, A. Tozeren, BMC Med. Imaging **6**, 14 (2006). doi:10.1186/1471-2342-6-14
7. P. Balasubramanian, L. Yang, J.C. Lang, K.R. Jatana, D. Schuller, A. Agrawal, M. Zborowski, J.J. Chalmers, Mol. Pharm. **6**, 1402 (2009). doi:10.1021/mp9000519
8. V. Nandakumar, L. Kelbauskas, K.F. Hernandez, K.M. Lintecum, P. Senechal, K.J. Bussey, P.C.W. Davies, R.H. Johnson, D.R. Meldrum, Plos One **7**, e29230 (2012). doi:10.1371/journal.pone.0029230
9. V. Nandakumar, L. Kelbauskas, R. Johnson, D. Meldrum, Cytom. Part A **79A**, 25 (2011). doi:10.1002/cyto.a.20997
10. T.C. George, D.A. Basiji, B.E. Hall, D.H. Lynch, W.E. Ortyn, D.J. Perry, M.J. Seo, C.A. Zimmerman, P.J. Morrissey, Cytometry A **59A**, 237 (2004). doi:10.1002/cyto.a.20048
11. T.C. George, S.L. Fanning, P. Fitzgeral-Bocarsly, R.B. Medeiros, S. Highfill, Y. Shimizu, B.E. Hall, K. Frost, D. Basiji, W.E. Ortyn, P.J. Morrissey, D.H. Lynch, J. Immunol. Methods **311**, 117 (2006). doi:10.1016/j.jim.2006.01.018
12. D.A. Basiji, W.E. Ortyn, L. Liang, V. Venkatachalam, P. Morrissey, Clin. Lab. Med. **27**, 653 (2007). doi:10.1016/j.cll.2007.05.008
13. V.P. Zharov, E.I. Galanzha, V.V. Tuchin, Opt. Lett. **30**, 628 (2005). doi:10.1364/OL.30.000628
14. V.P. Zharov, E.I. Galanzha, V.V. Tuchin, J. Biomed. Opt. **10**, 051502 (2005). doi:10.1117/1.2070167
15. V.P. Zharov, E.I. Galanzha, V.V. Tuchin, J. Cell Biochem. **97**, 916 (2006). doi:10.1002/jcb.20766
16. E.I. Galanzha, E.V. Shashkov, P.M. Spring, J.Y. Suen, V.P. Zharov, Cancer Res. **69**, 7926 (2009). doi:10.1158/0008-5472.CAN-08-4900
17. E.I. Galanzha, E.V. Shashkov, T. Kelly, J.W. Kim, L. Yang, V.P. Zharov, Nat. Nanotechnol. **4**, 855 (2009). doi:10.1038/nnano.2009.333
18. E.I. Galanzha, V.P. Zharov, Cancers (Basel) **5**, 1691 (2013). doi:10.3390/cancers5041691
19. D.A. Nedosekin, M.A. Juratli, M. Sarimollaoglu, C.L. Moore, N.J. Rusch, M.S. Smeltzer, V.P. Zharov, E.I. Galanzha, J. Biophoton. **6**, 523 (2013). doi:10.1002/jbio.201200242
20. E.M. Strohm, E.S.L. Berndl, M.C. Kolios, Photoacoustics **1**, 49 (2013). doi:10.1016/j.pacs.2013.08.003
21. E.M. Strohm, M.C. Kolios, Cytom. Part A **87**, 741 (2015). doi:10.1002/cyto.a.22698
22. E.M. Strohm, M.J. Moore, M.C. Kolios, IEEE J. Sel. Top. Quantum Electron. **22**, 6801215 (2016). doi:10.1109/JSTQE.2015.2497323
23. E.M. Strohm, E.S.L. Berndl, M.C. Kolios, Biophys. J. **105**, 59 (2013). doi:10.1016/j.bpj.2013.05.037
24. G.J. Diebold, T. Sun, M.I. Khan, Phys. Rev. Lett. **67**, 3384 (1991). doi:10.1103/PhysRevLett.67.3384
25. G.J. Diebold, M.I. Khan, S.M. Park, Science **250**, 101 (1990). doi:10.1126/science.250.4977.101
26. E. Moeendarbary, L. Valon, M. Fritzsche, A.R. Harris, D.A. Moulding, A.J. Thrasher, E. Stride, L. Mahadevan, G.T. Charras, Nat. Mater. **12**, 253 (2013). doi:10.1038/nmat3517
27. V.C. Anderson, J. Acoust. Soc. Am. **22**, 426 (1950). doi:10.1121/1.1906621
28. H.G. Frey, R.R. Goodman, J. Acoust. Soc. Am. **40**, 417 (1966). doi:10.1121/1.1910089
29. L.V. Wang, IEEE J. Sel. Top. Quantum Electron **14**, 171 (2008). doi:10.1109/JSTQE.2007.913398
30. G.J. Diebold, P.J. Westervelt, J. Acoust. Soc. Am. **84**, 2245 (1988). doi:10.1121/1.397017
31. G. Kino, *Acoustic Waves: Devices, Imaging, and Analog Signal Processing* (Prentice-Hall, New Jersey, 1997)
32. A. Siegman, *Lasers* (University Science Books, California, 1986)
33. M. Kolios, E. Strohm, G. Czarnota, in *Quantitative Ultrasound Soft Tissues*, ed. by J. Mamou, M. Oelze (Springer, Berlin, 2013), pp. 315–341
34. M.M. Pasternak, E.M. Strohm, E.S.L. Berndl, M.C. Kolios, Cell Cycle **14**, 2891 (2015). doi:10.1080/15384101.2015.1069925
35. H. Reile, G. Bernhardt, M. Koch, H. Schonenberger, M. Hollstein, F. Lux, Cancer Chemother. Pharmacol. **30**, 113 (1992). doi:10.1007/BF00686402
36. S.K. Arya, K.C. Lee, D.B. Dah'alan, Daniel, A.R.A. Rahman, Lab Chip **12**, 2362 (2012). doi:10.1039/C2LC21174B
37. D.L. Adams, P. Zhu, O.V. Makarova, S.S. Martin, M. Charpentier, S. Chumsri, S. Li, P. Amstutz, C.M. Tang, RSC Adv. **4**, 4334 (2014). doi:10.1039/C3RA46839A
38. J. Dahle, E. Kalanxhi, N. Tisnek, Anticancer Res. **31**, 2113 (2011)

39. I. Haque, S. Banerjee, A. De, G. Maity, S. Sarkar, M. Majumdar, S.S. Jha, D. McGragor, S.K. Banerjee, Oncogene **34**, 3152 (2015). doi:10.1038/onc.2014.250
40. B. Alberts, A. Johnson, J. Lewis, D. Morgan, M. Raff, K. Roberts, P. Walter, *Molecular Biology of the Cell*, 6th edn. (Garland Science, New York, 2015)
41. E.M. Strohm, V. Gnyawali, M. Van De Vondervoort, Y. Daghighi, S.S.H. Tsai, M.C. Kolios, Proc. SPIE **9708**, 97081A (2016). doi:10.1117/12.2211740